2-10-2017

Controlled Microfabrication of High-Aspect-Ratio Structures in Silicon at the Highest Etching Rates: The Role of H2O2 in the Anodic Dissolution of Silicon in Acidic Electrolytes

Chiara Cozzi
University of Pisa

Giovanni Polito
University of Pisa

Kurt W. Kolasinski
West Chester University of Pennsylvania, kkolasinski@wcupa.edu

Giuseppe Barillaro
University of Pisa

Recommended Citation
Cozzi, C., Polito, G., Kolasinski, K. W., & Barillaro, G. (2017). Controlled Microfabrication of High-Aspect-Ratio Structures in Silicon at the Highest Etching Rates: The Role of H2O2 in the Anodic Dissolution of Silicon in Acidic Electrolytes. *Advanced Functional Materials, 27*(6) http://dx.doi.org/10.1002/adfm.201770035

Controlled Microfabrication of High-Aspect-Ratio Structures in Silicon at the Highest Etching Rates: The Role of H_2O_2 in the Anodic Dissolution of Silicon in Acidic Electrolytes

C. Cozzi[1], G. Polito[1], K.W. Kolasinski[2], and G. Barillaro*[1]

[1] Dipartimento di Ingegneria dell'Informazione, Università di Pisa, via G. Caruso 16, 56122 Pisa, Italy

[2] Department of Chemistry, West Chester University, West Chester, PA 19383 USA

*g.barillaro@iet.unipi.it

ABSTRACT

In this work we report on the controlled electrochemical etching of high-aspect-ratio (from 10 to 100) structures in silicon at the highest etching-rates (from 3 to 10 μm/min), at room temperature. This allows silicon microfabrication entering a previously unattainable region where etching of high aspect ratio structures (beyond 10) at high etching rate (over 3 μm/min) was prohibited for both commercial and research technologies. Addition of an oxidant, namely H_2O_2, to a standard aqueous HF electrolyte is used to dramatically change the stoichiometry of the silicon dissolution process under anodic biasing without loss of etching control accuracy at the higher depths (up to 200 μm). We show that the presence of H_2O_2 reduces the valence of the dissolution process to 1, thus rendering the electrochemical etching more effective, and catalyzes the etching rate by opening

a more efficient path for silicon dissolution with respect to the well-known Gerischer mechanism, thus increasing the etching speed at both shorter and higher depths.

Keywords: silicon microfabrication, electrochemical etching, anodic dissolution, high etching speed, high aspect ratio, hydrogen peroxide

INTRODUCTION

Since the famous talk of R. Feynman in 1959 “There is plenty of room at the bottom”, silicon microstructuring technologies have been continuously developed with the ambition of sculpting silicon at the microscale, thus pushing silicon towards novel research topics and market opportunities beyond Moore's law, a trend also known as More Than Moore [1, 2]. As a result, silicon microoptoelectromechanical systems (MOEMS) (e.g. pressure sensors, accelerometers, gyroscopes) are nowadays an integral component of virtually any of the sophisticated devices (e.g. mobile phones, cars, videogames, airplanes) of everyday life [3-5]. On the other hand, lab-on-a-chip systems integrating a multitude of micrometer-sized components on a silicon chip (e.g. microneedles, microchannels and valves, biosensors) are on the way and will radically transform clinical diagnostics and medicine [6, 7]. Finally, emerging applications in microelectronics, e.g. Through Silicon Vias (TSV) for 3D chip stacking and 3D capacitors (HVC) with dramatically enhanced value for unit area, are among the new critical challenges that silicon microstructuring technologies are facing today [8, 9]. Both these applications require the development of novel high-aspect-ratio structures that are well beyond values attainable by commercial technologies

(AR<40). On the other hand, state-of-the-art technologies able to control microfabrication at higher aspect-ratios (AR>100) are limited in terms of etching rate, which is usually restricted to below 2 μm/min when the aspect-ratio increases over 20.

Figure 1 groups experimental data on growth rate versus aspect ratio value typical of the principal commercial and research microfabrication technologies, according to authors' best knowledge. Prior results define an unattainable region that is inaccessible for silicon microfabrication technologies, either at commercial or research level (gray area in Fig. 1). Its boundary is quite reasonably well described by a power law $GR=a\ AR^b$, as estimated from experimental data available on the different microfabrication technologies, where GR is the growth rate in μm/min, AR is the aspect-ratio, and *a* and *b* are fitting parameters (*a*=23.9 and *b*=-0.55 on the basis of data available on Fig. 1).

Time-multiplexed etching (TMEP) process, also known as Bosch process, is the leading microfabrication technology at industrial level [10]. It relies on alternating etching and passivation (polymerization) steps, e.g. using SF_6 as etch gas and CHF_3 and Ar as polymerization gases. In spite of TMEP being highly reliable and greatly flexible, TMEP features an aspect ratio dependent etching rate (ARDE) [11]. ARDE usually limits AR of microfabricated pores in the range from 1 to16 at etching rates from 6 to 3 μm/min, respectively (black stars in Figure 1). Although ARDE is less restrictive for trenches, their aspect ratio is also limited to a maximum value of 21 at etching rate of about 4 μm/min (green squares in Figure 1).

Metal assisted chemical etching (MACE) is a novel microfabrication technology that allows targeting AR of 30 though at etching rate <1 μm/min (red upside-down triangles in Figure 1) [12, 13]. MACE makes use of HF-H_2O_2 solutions to catalyze chemical silicon dissolution in correspondence with noble metal (e.g. Pt, Au) sites patterned on the silicon surface. Although largely used at research level, the low etching rate (about 10 times lower that TMEP processes) hinders MACE application to large-scale manufacturing. An electric bias-attenuated metal-assisted chemical etching (EMaCE) was recently reported that enhances the etching rate of MACE to 11.3 μm/min at AR of 4 (cyan diamonds in Figure 1) [14]. EMaCE exploits electrical biasing of the silicon substrate to focus holes responsible for initiation of silicon dissolution underneath the metal catalyst, thus improving both etching control and speed. Still, the EMaCE etching rate decreases rapidly with aspect ratio, with a value of about 2.7 μm/min at AR of 11.

Silicon electrochemical etching (ECE) is a well-known technology for microfabrication of both ordered pores [15, 16] and complex systems [17, 18]. Back-side illumination is used to focus holes specifically to defects patterned on the surface of *n*-type silicon wafers and enable, in turn, controlled dissolution in aqueous HF (5% by vol.) electrolytes under anodic biasing. AR values over 100 are obtained for ordered pores and systems with micrometric features, though the etching (about 2 μm/min at low AR) reduces to 0.5 μm/min at the highest ARs (blue circles in Figure 1). Increasing the HF concentration from 5 to 10% (by vol.) allowed maintaining the etching rate constant at 2.2 μm/min regardless of the AR value, in the range from 17 to 88 (orange hexagrams in Figure 1) [19]. However, only pore fabrication (no microstructures) has been demonstrated with such an increased HF concentration.

Summarizing, silicon technologies, either wet or dry, are strongly limited by diffusion of reactive species within narrow and deep pores, which limits the fabrication of high AR pores at high etching rate. Diffusion of chemical species within the pores (i.e. Fick's law) as well as removal of reaction byproducts from the pores are responsible for such a reduced etching rates as AR increases. A necessary trade-off among concentration of reactive species, removal of chemical byproducts, and flexibility and control on the etching process has set this boundary so far.

In this work we report on a micromachining technology able to enter the previously unattainable region in Figure 1 (cyan triangles). More in detail, we enable the controlled electrochemical etching of high-aspect-ratio (from 10 to 100) structures in silicon at the highest etching-rates (from 3 to 10 μm/min), at room temperature using a low HF concentration (5% by vol). This sets a novel record among either commercial or state-of-art silicon etching technologies. We show that the addition of an oxidant, namely H_2O_2, to a standard aqueous HF electrolyte facilitates a dramatic change in the stoichiometry of the silicon dissolution process under anodic biasing without loss of etching control accuracy at the higher depths (up to 200 μm). The presence of H_2O_2 acts both in dropping the valence of the silicon dissolution process to 1, thus rendering the electrochemical etching more effective, and in catalyzing the etching rate by opening a more efficient path for silicon dissolution with respect to the well-known Gerischer mechanism [20, 21], thus increasing the etching speed at both shorter and higher depths.

RESULTS AND DISCUSSION

Controlled high-speed electrochemical etching at high-aspect-ratio of regular macropores and microstructures in *n*-type silicon in aqueous HF-H_2O_2 electrolytes

Figure 2 shows SEM cross-section images of regular arrays of macropores electrochemically etched under back-side illumination at anodic voltage of 1.2 V in two aqueous electrolytes containing [HF] = 5% with H_2O_2 at concentration of 25% (Figure 2a,c) and without H_2O_2 (used as control) (Figure 2b,d), at two etching times, namely 10 and 60 minutes. The control electrolyte (without H_2O_2) was a well-known mixture of HF:H_2O (5%:95% by vol) commonly employed for the electrochemical etching of both regular macropores [15] and complex microstructures [17, 18] in *n*-type silicon electrodes at low anodic voltage under back-side illumination. Remarkably, macropores etched for 10 min in the electrolyte with [H_2O_2] = 25% feature a mean depth of 48.99 μm (sd = 0.07 μm), which corresponds to an average etching rate over 10 minutes of about 5 μm/min. The average etching rate with [H_2O_2] = 25% was about 2.8 times larger than that of the control electrolyte (without H_2O_2) for which shorter macropores with depth of only 18.45 μm (sd = 0.25 μm) were etched in the same time (about 1.8 μm/min), in agreement to the current literature [22]. By increasing the etching time to 60 minutes, macropores with mean depth of 177.93 μm (sd = 0.37 μm) were etched using the electrolyte with [H_2O_2] = 25%, whereas macropores etched with the control electrolyte feature a mean depth of 90.38 μm (sd = 0.59 μm). The average etching rate over 60 minutes in the electrolyte with [H_2O_2]=25% was about 3 μm/min, which was about 2 times larger than that in the control

electrolyte (about 1.5 μm/min). It is important to note that the etching rate was evaluated as the ratio between etch depth and etch time. On the basis of these experimental results, we can assert that the presence of $[H_2O_2]$ = 25% in the electrolyte during silicon electrochemical etching facilitates significant enhancement of the silicon etching rate and, in turn, macropore growth rate, at any depth with respect to the control electrolyte (without H_2O_2). Nonetheless, reduction in the etching rate from about 5 μm/min at a depth of about 50 μm to about 3 μm/min at a depth of about 180 μm clearly indicates that the diffusion kinetics of active species, i.e. HF and H_2O_2, to the active site of reaction, i.e. the macropore tip, still plays a major role in the electrochemical dissolution of silicon over depth [15, 22].

Remarkably, the enhancement of the etching rate in the presence of H_2O_2 does not negatively affect macropore quality (e.g. in terms of surface roughness, pore diameter, or their dependence on depth) with respect to macropores etched in control electrolyte. From SEM analysis of macropore cross-sections no appreciable difference in both surface roughness and diameter variation (over depth) was observed in the presence of H_2O_2 with respect to the reference solution. Moreover, the peculiarity of the electrochemical etching technology enabling fabrication of complex microstructures at high AR value with high accuracy by modulation in real-time of the etching anisotropy [17, 18] is also retained at such high etching rates. Figure 2e,f shows SEM bird-views of a silicon microstructure that integrates a 2D array of square holes with sides of about 40 μm and spatial periods of 70 μm together with a 2D array of square pores with sides of about 4 μm and spatial periods of 10 μm. Both arrays feature a depth of about 50 μm after an etching time of 10 minutes in a [HF]=5% electrolyte with $[H_2O_2]$=25%. An etching time of 35 minutes is needed to fabricate the same microstructure using

the standard electrolyte [24]. The etching depth is in good agreement with depth of regular macropore arrays in Figure 1a. The microstructure combines on the same die low (about 1) and high (about 10) AR holes etched at an average rate of 5 μm/min.

To gain insight on the effect of addition of H_2O_2 to the control electrolyte on the silicon dissolution process, regular macropore etching in *n*-type silicon under back-side illumination was investigated for different H_2O_2 concentrations ([H_2O_2] = 0, 5, 10, 20, 25%) as a function of the etching time (from 0 to 65 min, step 10 min). Regardless of the electrolyte composition, all experiments were carried out with the same initial etching parameters, and etching current density was adjusted over time to keep the pore diameter constant over depth, as detailed in the Materials and Methods section. For a given H_2O_2 concentration an experimental growth curve linking macropore depth and etching time was recorded by using a labeling methodology. This latter method allows marking the macropore growth over time on a single silicon sample using a time-pulse modulation of the etching current density (Figure S1a), as detailed in Supporting Information. Preliminary experiments were carried out with the control electrolyte and with an electrolyte containing [H_2O_2] = 5% aimed at validating the effectiveness of the labeling methodology with respect to the standard methodology, for which a new experiment is required for any different etching time. Outcomes of these experiments (Figure S1) confirm that pore growth curves obtained by using the two methodologies are identical within the experimental error (Figure S1c).

Figure 3a shows experimental growth curves (mean value and standard deviation) of regular macropores electrochemically etched in *n*-type silicon under back-side illumination up to 65 minutes using aqueous HF-based electrolytes without (control) and with H_2O_2 at concentrations in the range from 5 to 25% (by vol.).

From Figure 3a it is immediately apparent that: 1) for any tested electrolyte the pore depth consistently increased with etching time; 2) for any etching time the etching depth consistently increased with H_2O_2 concentration in the electrolyte. The growth curves for both control electrolyte and electrolyte with $[H_2O_2] = 25\%$ are in good agreement with the results of experiments reported in Figure 2. The higher H_2O_2 concentration in the electrolyte enabled the etching of about 200-μm-deep regular macropores with aspect-ratio of about 100 in roughly 1 hour, thus breaking new ground in the silicon micromachining arena. For comparison, etching of regular macropores with the same depth using reference electrolyte takes about 4 hours.

Figure 3b shows experimental data on the growth rate (in μm/min) versus depth of regular macropores as a function of the H_2O_2 concentration in the electrolyte. It is apparent that the control electrolyte ($[H_2O_2] = 0\%$) has a maximum growth rate of about 2 μm/min for smaller etching depth (<20 μm) that decreases with depth due to HF diffusion within the pores and tends to a limiting value below 1 μm/min at higher etching depth (>80 μm), in agreement to literature data [23]. Conversely, by increasing the concentration of H_2O_2 in the electrolyte it is possible to monotonically and significantly increase the growth rate both at the smaller and higher depth, with respect to the reference electrolyte (Figure S2a,b). Indeed, at smaller depth (≤20 μm) the macropore growth rate is higher than 7 μm/min and decreases to about 3 μm/min at higher etching depth (≥200 μm), in the presence of $[H_2O_2] = 25\%$. Figure S2c highlights the significant increase of the growth rate versus aspect ratio of etched pores in the presence of H_2O_2. As the H_2O_2 in the electrolyte increases, there is a dramatic increase of the growth rate for any aspect ratio, with respect to the reference electrolyte. It is worth noting that: 1) addition of $[H_2O_2] = 5\%$ to the control electrolyte is enough to roughly double the

macropore growth rate both at the smaller and higher depth, with respect to the control electrolyte itself; 2) addition of $[H_2O_2]$ = 10, 20 and 25% to the control electrolyte allows increasing the macropore growth rate respectively 2.7, 3.6 and 4 times at the smaller depth, and 2, 2.2 and 2.4 times at the higher depth, with respect to the control electrolyte itself; 3) electrolytes containing H_2O_2 feature a growth rate at the higher depth that is always higher than that of the control electrolyte in spite of the lower depth of macropores etched for the latter, regardless of the H_2O_2 concentration.

To gain a deeper understanding of the effect of H_2O_2 on the electrochemical dissolution of silicon in HF-aqueous electrolytes, the diameter of etched ordered macropores (Figure 3c) and dissolution valence of electrochemical etching process (Figure 3d) were investigated as a function of the H_2O_2 concentration. The diameter of macropores etched in electrolyte with $[H_2O_2]$ = 25% had an average value of 1.99 μm (sd = 0.18 μm), whereas macropores etched in the control electrolyte featured an average diameter of 3.05 μm (sd = 0.19 μm), which was about 1.5 times larger and in agreement with literature data [25]. This means that the presence of $[H_2O_2]$ = 25% in the electrolyte during anodic dissolution of silicon enhances macropore growth rate in the out-of-plane direction with respect to the in-plane direction, if compared with control electrolyte, which is consistent with the etching of deeper macropores with smaller diameter.

The dissolution valence n, by definition the number of charge carriers required for the dissolution of a single silicon atom, of the electrochemical etching process in the presence of $[H_2O_2]$ = 25% had an average value of 1.12 (sd = 0.24), whereas the dissolution valence with the reference electrolyte had an average diameter of 2.97 (sd = 0.40), which is in good agreement with literature data [23].

Remarkably, the dissolution valence decreased as the H_2O_2 concentration in the

electrolyte increased, thus corroborating the hypothesis that the oxidant agent, namely H_2O_2, was able to promote a change in the stoichiometry of silicon dissolution process by consuming conduction band electrons [26].

Current density-voltage curves of *n*-type silicon electrodes in aqueous HF-H_2O_2 electrolytes

Figure 4a,b shows typical experimental current density-voltage (*J-V*) curves (average value and standard deviation) of *n*-type silicon electrodes in the presence of the two electrolytes with the same [HF] = 5% though different [H_2O_2], namely 25% (Figure 5a) and 0% (control) (Figure 5b). The *J-V* curves were recorded around the OCP region between -1 and +2.5 V at different illumination intensity values obtained by tuning the lamp power from 0 to 100%. The *J-V* curves mostly refer to the anodic region of the silicon/electrolyte system, because silicon dissolution in HF-based electrolytes only occurs under anodic biasing. *J-V* curves referring to the other electrolytes under investigation, with H_2O_2 concentration between 5 and 20%, are reported in Supporting Information (Figure S3).

From the *J-V* curves of Figure 4a,b it is apparent that, regardless of the presence of H_2O_2, the silicon/electrolyte system was reverse-biased under anodic voltage and the use of back-side illumination of the silicon electrode allowed for fine control of the etching current density flowing through the silicon/electrolyte junction.

In dark condition (red curves in Figure 4a,b) only a small current density flowed through the silicon/electrolyte junction, with an average value increasing with the

H_2O_2 concentration, from 3.7 μA/cm^2 (sd = 0.8 μA/cm^2) in the control electrolyte to 26.1 μA/cm^2 (sd = 1.1 μA/cm^2) for the electrolyte with [H_2O_2] = 25 % (Figure 4c). The current density value recorded in dark condition with the control electrolyte (without H_2O_2) was in good agreement with data reported in the literature [27, 28]: the slow charge injection from fluoride ions (F^-) during silicon etching determined its low value. The addition of different concentrations of H_2O_2 to the control electrolyte increased current density values in dark and, in turn, charge injection by a factor of 7 (Figure 4c), though its value was still extremely low in comparison with charge injection recorded under back-side illumination (from blue to black curves in Figure 4a). We argue that the direct charge injection from H_2O_2 into the Si valence band makes a negligible contribution to the current that flows during etching.

Under illumination of the silicon electrode (blue, green, magenta, and black curves in Figure 4a,b), the electrical current flowing through the silicon/electrolyte junction significantly increased thanks to the contribution of holes photo-generated at the back-side silicon surface and collected at the silicon/electrolyte interface. Under high illumination intensity (≥50% of the lamp power), a typical electropolishing current density peak J_{ep} = 66.45 mA/cm^2 at anodic voltage of V_{ep} = 1 V was clearly visible with the control electrolyte (Figure 4b), beyond which the current density increased almost linearly with anodic voltage [16]. Conversely, as the H_2O_2 concentration in the control electrolyte increased from 5 to 25%, on the one hand, the electropolishing current density peak did not show up anymore (being already barely visible with 5% of H_2O_2) and the current density linearly increased with the anodic voltage until saturation (Figure 4a and Figure S3a-c); on the other hand, under high illumination intensity

(≥50% of the lamp power) the slope of the current density-voltage curves (d*J*/d*V*) decreased as the H_2O_2 concentration increased (Figure S3d), thus confirming that H_2O_2 was unable to significantly inject charges into silicon during etching.

We argue in the next section that the ability of the oxidant (i.e. H_2O_2 in this case) to change the stoichiometry of anodic silicon dissolution is related to its ability to consume the conduction band electrons produced in the second step of the well-known Gerischer mechanism [26]. It can also explain the reduction of the current density-voltage curves slope (d*J*/d*V*) as H_2O_2 concentration increased: H_2O_2 molecules scavenge conduction band electrons, which are then not measured, to generate hydroxide ions (OH^-), well known to catalyze the reaction of H_2O with silicon [29, 30].

The OCP value was also dependent on the presence of H_2O_2 in the electrolyte, both in dark and under illumination conditions, as shown in Figure 4d. In dark condition, the OCP value exhibited a clear cathodic shift in the presence of H_2O_2, from -0.5 V (sd = 0.05 V) for the reference electrolyte to -1 V (sd = 0.09 V) for the electrolyte with [H_2O_2] = 25%, with no significant dependence on the H_2O_2 concentration. Under illumination, the OCP value showed an anodic shift with respect to dark condition, from -0.5 V (sd = 0.05 V) to -0.325 V (sd = 0.05 V) for the reference electrolyte and from -1 V (sd = 0.09 V) to -0.5 V (sd = 0.0005 V) for the electrolyte with [H_2O_2] = 25%, in agreement with the literature [31]. Moreover, under illumination, the OCP value exhibited a cathodic shift as H_2O_2 concentration increased in the electrolyte, from -0.325 V of the reference electrolyte (OCP_0) to -0.5 V for the electrolyte with [H_2O_2] = 25% (OCP_{25}). The cathodic OCP shift value ($\Delta OCP = OCP_{25} - OCP_0$) is equal to -0.175 V, which means that the Fermi level is shifting up in energy by +0.175 V. We argue that

addition of H_2O_2 lowers the band bending of 0.175 V in silicon/electrolyte band diagram, in good agreement with the literature [32].

Dissolution mechanism of *n*-type silicon in aqueous HF- H_2O_2 electrolytes

We have demonstrated that the rate of anodic etching in acidic fluoride solutions is enhanced by the presence of H_2O_2 in the electrolyte. In the previous section we proposed that this enhancement involves the capture of conduction band electrons by H_2O_2. In this section we describe this enhancement mechanism. The mechanism is depicted schematically in Figure 5.

In the absence of H_2O_2, anodic etching of Si in acidic fluoride solutions occurs by the Gerischer mechanism [21], which can occur along a dominant valence 2 pathways and a less likely valence 4 pathway [22, 33]. Therefore, the effective valence during pore formation is usually measured to be slightly above 2. There also is a valence 4 oxidation pathway that contributes to electropolishing at high current density [16, 32]. The valence 2 pathway is depicted in Figure 5. Etching is initiated by hole injection into the Si valence band at the top of the figure. In step 2, a fluoride ion injects an electron into the conduction band. This "doubling electron", when measured in conjunction with the hole injected in step 1, accounts for the valence of 2. It has been shown that the balance between the valence 2 and valence 4 pathways can be altered by the reaction conditions; for example, metal catalysts induce etching with valences between 2 and 4 depending on the chemical identity of the metal [35, 36].

Even though H_2O_2 has a standard reduction potential ($E° = 1.775$ V) that lies far below the Si valence band maximum ($E° \sim 0.7$ V), it is unable to inject holes into

the valence band at an appreciable rate compared to the rates of anodic dissolution. This is consistent both with the results we have presented above and with literature reports [29, 30, 37]. The reason for this is that H_2O_2 couples very weakly to the electronic states of the Si valence band. Therefore, specific adsorption and the presence of catalytic metals are required for rapid electron transfer [35, 36].

We propose that the manner in which H_2O_2 enhances the rate of anodic dissolution is not via direct electron transfer from the valence band. Instead, the H_2O_2 enhances the etching rate by capturing the doubling electron, which resides in the conduction band. As shown in the left hand side of Figure 5, the capture of a conduction band electron will generate OH^-. Hydroxide is well known to catalyze the etching of Si by H_2O [29, 30]. While this normally only occurs at high pH, in the mechanism proposed here OH^- is generated directly on the Si surface. Furthermore, the consumption of the doubling electron by the H_2O_2 means that the effective valence in the presence of both the right hand and left hand pathways will be measured as 1. Both pathways are initiated by hole injection into the valence band but neither can proceed without the adsorption of F^- and the concomitant injection of an electron into the conduction band.

MATERIALS AND METHODS

Materials and Chemicals

The starting material is a CZ-growth *n*-type silicon wafer with resistivity of 3-8 Ω•cm, (100) oriented, phosphorous-doped, with a 298-nm-thick silicon-dioxide layer on top, provided by ST microelectronics.

Hydrofluoric acid (HF) 48% wt, Perdrogen™ H_2O_2 30% wt, pentane ($CH_3(CH_2)_3CH_3$) 99% wt, acetone (CH_3COCH_3) 99% wt and 2-Propanol ($(CH_3)_2CHOH$) 99.8% wt are purchased from Sigma-Aldrich. Sodium lauryl sulphate (SLS) powder ($CH_3(CH_2)_{11}OSO_3Na$) is purchased from Carlo Erba Reagents. Potassium hydroxide (KOH), pure powder at 85%, and ethanol (CH_3CH_2OH) 99.8% wt are purchased from Fluka Analytical. Ammonium fluoride solution (NH_4F) 40% wt is purchased from Riedel-De Haën (Aldrich).

Electrochemical characterization of *n*-type silicon electrode in aqueous HF-H_2O_2 electrolytes by linear sweep voltammetry

Linear sweep voltammetry on *n*-type silicon electrodes in contact with aqueous HF-based electrolytes ([HF]=5% by vol) containing different H_2O_2 concentrations (namely 0% (reference), 5, 10, 20, and 25% by vol) was carried out at voltages from -1 to +2.5 V, around the open-circuit-potential (OCP), under back-side illumination of the silicon at different intensity values (from 0 to 100% power of a 250 W halogen lamp). The silicon-dioxide layer on top of the silicon wafer was removed by chemical etching in HF:ethanol (1:1 by vol.) before the silicon was loaded in a three-electrode electrochemical cell. Details of the electrochemical cell are provided in the Supporting Information. The current density-voltage (*J*-*V*) curve of the electrochemical systems under investigation was recorded by monitoring the current flowing through silicon electrode (used as the anode) and the counter electrode (i.e. a platinum disk) after applying a variable voltage in the range from +2.5 to -1 V with sweep rate of -0.1 V/s between the silicon electrode and a pseudo-reference electrode (i.e. a platinum wire). A set of three measurements was carried out for each parameter configuration.

Preparation of regular macropores in *n*-type silicon electrode in aqueous HF-H_2O_2 electrolytes by galvanostatic anodic etching

A square hole array oriented along the (110) direction with side-to-side pitch of 3.5 μm was defined on the surface of the silicon wafer. Standard UV lithography was used to define the pattern on positive photoresist layer deposited on the silicon-dioxide surface on top of the *n*-type silicon wafer. The pattern was then transferred to silicon-dioxide layer by buffered hydrofluoric acid (BHF) etching using the patterned photoresist as a mask. BHF etching was performed at room temperature with a solution of HF:NH_4F (4:25 by vol). The positive photoresist layer was removed by chemical dissolution in acetone, then the pattern was transferred to the silicon surface by potassium hydroxide (KOH) etching using the silicon-dioxide layer as mask, so as to create an array of inverted pyramid-shaped defects. KOH etching was performed at 50 °C in a 20% KOH solution saturated with 2-propanol to improve solution wettability and, in turn, to increase the etching uniformity. The silicon-dioxide layer was removed by chemical etching in a solution of HF:ethanol (1:1 by vol.), thus leaving the patterned silicon surface uncovered. The patterned silicon samples were loaded in a three-electrode electrochemical cell and electrochemically etched under back-side illumination at constant anodic voltage of 1.2 V for different etching times, namely 10, 20, 40, and 60 s, in the presence of five different aqueous electrolytes with same HF concentration ([HF]=5% by vol) though different H_2O_2 concentration, namely $[H_2O_2]$ = 0% (reference), 5, 10, 20, and 25% (by vol). In order to keep the macropore diameter constant as a function of depth, the photogenerated etching current density (J_e) was linearly decreased over time with respect to its initial

value J_{e_0} = 36.49 mA/cm^2, which was maintained constant regardless of the electrolyte composition. Accordingly, the lamp power was reduced over time to set the decreasing rate value to -1.67 μA/s for the reference solution, -1.67 μA/s for the electrolyte with [H_2O_2] = 5%, -3.44 μA/s for the electrolyte with [H_2O_2] = 10%, -4.04 μA/s for the electrolyte with [H_2O_2] = 20%, and -4.04 μA/s for the electrolyte with [H_2O_2] = 25%. The macropore growth versus time was investigated using two different methodologies: 1) a standard methodology, which required performing a number of experiments equal to the number of etching times/depths (i.e. 10, 20, 40, and 60 min) to be investigated; 2) a labeling methodology, which required performing a single experiment at the higher etching time to be investigated (i.e. 65 min) during which depth was marked over time at specific time intervals [22]. Details on the labeling methodology used in this work are provided in Supporting Information. After the electrochemical etching the micro-fabricated silicon samples were rinsed in deionized water, ethanol, and pentane, then dried on a hotplate at 100 °C and diced in two pieces along the (100) direction to allow morphological investigation of cross-sections.

Preparation of microstructures in *n*-type silicon electrode in aqueous HF-H_2O_2 electrolytes by galvanostatic anodic etching

Silicon microstructures integrating a 2D array of square holes with sides of about 40 μm and spatial periods of 70 μm together with a 2D array of square pores with sides of about 4 μm and spatial periods of 10 μm were pre-patterned on the surface of silicon samples according to technological steps detailed in section 2.3. The larger holes were partitioned with sacrificial structures consisting of basic

elements (i.e., a straight line with a suitable length of 36 μm and width 2 μm) arranged as 1D arrays of parallel lines and designed to become free-standing at the end of the electrochemical etching step. The patterned silicon samples were loaded in a three-electrode electrochemical cell and electrochemically etched under back-side illumination at constant anodic voltage of 3 V for 10 minutes in in an aqueous electrolyte with same [HF]=5% (by vol) with [H_2O_2] = 25% (by vol).

The electrochemical etching consisted of a single step with an initial anisotropic phase and a final isotropic phase, both controlled by varying the etching current density (J_e) as the etching progresses [17]. During the anisotropic etching phase the pattern is deeply grooved into the silicon substrate. In this phase the J_e value was set to 103.9 mA/cm^2 and gradually decreased over time with a slope of -11.7 μA/s for the next 10 minutes. During the isotropic etching phase, only silicon at the bottom the anisotropically-etched structure is etched. In this phase the J_e value was abruptly brought to a constant value of 148.4 mA/cm^2 for 90 s so as to fully consume silicon at the bottom of sacrificial structures, which are then removed from inside the larger holes.

Investigation of morphological features of regular macropores and microstructures

Optical (Leica Microsystems DFC295) and scanning electron (SEM JEOL JSM-6390 at an acceleration voltage of 3kV) microscopy are used to investigate both top-view and cross-section of electrochemically-etched macropore arrays and

microstructures in order to probe both depth and diameter as a function of etching time and electrolyte composition.

Calculation of the dissolution valence of the electrochemical etching process

The number of charge carriers required for the dissolution of a single silicon atom, by definition dissolution valence n, is estimated from experimental data on regular macropore etching according to the following equations:

$$n = \frac{N_c}{N_{Si}} \quad \text{(Eq.1)}$$

$$N_c = \frac{A_e \cdot t_e}{2 \cdot e}\left(J_{e\_0} + J_{e\_end}\right) \quad \text{(Eq.2)}$$

$$N_{Si} = V_{Si} \cdot \rho_{Si} \quad \text{(Eq.3)}$$

where N_c is the number of charge carriers supplied to the silicon/electrolyte system during the etching process; J_{e_0} and J_{e_end} [mA/cm^2] are initial and final etching current density values, respectively, used for each tested electrolyte (as detailed in Section 2.3); A_e [cm^2] is the area under etching of the silicon electrode; t_e [s], is the etching time; e [C] is the electron charge; N_{Si} is the total number of the silicon atoms removed during the etching; V_{Si} [μm^3] is the volume of silicon removed during the etching, and ϱ_{Si} [atom/μm^3] is the silicon atomic density.

4. CONCLUSIONS

We demonstrate that the rate of macropore formation by the anodization of Si in HF solutions is dramatically enhanced by the addition of H_2O_2. The enhancement facilitates the machining of structures into Si at rates that were previously unattainable. More importantly, higher etching rates are maintained during the

formation of high-aspect-ratio structures compared to processes that are considered to be state-of-the-art. The rate enhancement is accompanied by a drop of the effective reaction valence to a value of 1. We propose that a parallel etching mechanism introduced by the addition of H_2O_2 is triggered by the capture of a conduction band electron released during fluoride-induced etching. This parallel pathway is responsible both for the rate enhancement and the reduction in effective valence.

REFERENCES

1. Lundstrom, M. Moore's law forever? *Science* **299,** 210 (2013).

2. Waldrop, M. M. The chips are down for Moore's law. *Nature* **530,** 144-147 (2016).

3. Monat, C., Domachuk, P. & Eggleton, B. J. Integrated optofluidics: a new river of light. *Nat. Photon.* **1,** 106-114 (2007).

4. Krause, A. G., Winger, M., Blasius, T. D., Lin, Q. & Painter, O. A high-resolution microchip optomechanical accelerometer. *Nat. Photon.* **6,** 768-772 (2012).

5. Coarer, E. L. E. et al. Wavelength-scale stationary-wave integrated Fourier-transform spectrometry. *Nat. Photon.* **6,** 473-478 (2007).

6. Dittrich, P. S. & Manz, A. Lab-on-a-chip: microfluidics in drug discovery. *Nat. Rev. Drug Discov.* **5,** 210-218 (2006).

7. Neužil, P., Giselbrecht, S., Länge, K., Huang, T. J. & Manz, A. Revisiting lab-on-a-chip technology for drug discovery. *Nat. Rev. Drug Discov.* **11,** 620-632 (2012).

8. Fischer, A. C. et al. Integrating MEMS and ICs. *Microsystems & Nanoengineering* **1,** (2015).

9. Gibb, K. & Krishnamurthy, R. Drilling and filling, but not in your Dentist's chair - a look at some recent history of multi-chip and through silicon via (TSV) technology. *Chip Design* 29-32 (2008).

10. Banqiu, W., Kumar, A. & Pamarthy, S. High aspect ratio silicon etch: a review. *J. Appl. Phys.* **108,** (2010); and reference within it.

11. Junghoon,Y., Wu, Y., Selby, J. C. & Shannon, M. A. Maximum achievable aspect ratio in deep reactive ion etching of silicon due to aspect ratio dependent transport and the microloading effect. *J. Vac. Sci. & Technol., B* **23,** 2319 (2005).

12. Zhipeng, H., Geyer, N., Werner, P., De Boor, J. & Gösele, U. Metal-assisted chemical etching of silicon: a review. *Adv. Mater.* **23,** 285-308 (2011).

13. Chang, S.-W., Chuang, V. P., Boles, S. T., Ross, C. A. & Thompson, C. V. Densely packed arrays of ultra-high-aspect-ratio silicon nanowires fabricated using block-copolymer lithography and metal-assisted etching. *Adv. Funct. Mater.* **19,** 2495-2500 (2009).

14. Chang, C. & Sakdinawat, A. Ultra-high aspect ratio high-resolution nanofabrication for hard X-ray diffractive optics. *Nat. Commun.* **5,** 1–7 (2014).

15. Li, L., Zhao, X. & Wong, C.-P. Deep etching of single- and polycrystalline silicon with high speed, high aspect ratio, high uniformity, and 3D complexity by electric bias-attenuated metal-assisted chemical etching (EMaCE). *ACS Appl. Mater. Interfaces* **6,** 16782-16791 (2014).

16. Lehmann, V. *Electrochemistry of Silicon*. Wiley-VCH, (2002).

17. Barillaro, G. & Strambini, L. M. Controlling macropore formation in patterned n-type silicon: existence of a pitch-dependent etching current density lower bound. *Electrochem. Commun.* **12,** 1314-1317 (2010).

18. Bassu, M., Surdo, S., Strambini, L. M. & Barillaro, G. Electrochemical micromachining as an enabling technology for advanced silicon microstructuring. *Adv. Funct. Mater.* **22,** 1222-1228 (2012).

19. Surdo, S. et al. Optofluidic microsystems with integrated vertical one-dimensional photonic crystals for chemical analysis. *Lab Chip* **12,** 4403-4415 (2012).

20. Cojocaru, A. et al. Fast macropore growth in n-type silicon. *Phys. Status Solidi, C* **6,** 1571-1574 (2009).

21. Gerischer, H., Allongue, P. & Kieling, V. C. The mechanism of the anodic oxidation of silicon in acidic fluoride solutions revisited. *Ber. Bunsenges. Phys. Chem.* **97,** 753 (1993).

22. Kolasinski, K. W. Etching of silicon in fluoride solutions. *Surf. Sci.* **603,** 1904-1911 (2009).

23. Barillaro, G. & Pieri, F. A self-consistent theoretical model for macropore growth in n-type silicon. *J. Appl. Phys.* **97,** 8-11 (2005).

24. Polito, G. et al. Two-dimensional array of photoluminescent light sources by selective integration of conjugated luminescent polymers into three-dimensional silicon microstructures. *Adv. Opt. Mater.* **1,** 894-898 (2013).

25. Lehmann, V. The physics of macropore formation in low doped n-type silicon. *J. Electrochem. Soc.* **140,** 2836-2843 (1993).

26. Kolasinski, K. W. & Barclay, W. B. The stoichiometry of electroless silicon etching in solutions of V_2O_5 and HF. *Angew. Chem. - International Edition* **52,** 6731-6734 (2013).

27. Halimaoui, A. Determination of the specific surface area of porous silicon from its etch rate in HF solutions. *Surf. Sci.* **306,** (1994).

28. Wang, J. et al. A comparative Raman spectroscopy study on silicon surface in HF, HF/H_2O_2 and HF/NH_4F aqueous solutions. *Mat. Sci. Eng., B* **72,** 193-196 (2000).

29. Hines, M. A., Chabal, Y. J., Harris, T. D. & Harris, A. L. Measuring the structure of etched silicon surfaces with Raman spectroscopy. *J. Chem.Phys.* **101,** 8055 (1994).

30. Baum, T. & Schiffrin, D. J. Mechanistic aspects of anisotropic dissolution of materials etching of single-crystal silicon in alkaline solutions. *J. Chem. Soc. Faraday Trans.* **94,** 691-694 (1998).

31. Bertagna, V., Plougonven, C., Rouelle, F. & Chemla, M. p- and n-type silicon electrochemical properties in dilute hydrofluoric acid solutions. *J. Electrochem. Soc.* **143,** 3532-3538 (1996).

32. Philipsen, H. G. G. & Kelly, J. J. Influence of chemical additives on the surface reactivity of Si in KOH solution. *Electrochim. Acta* **54,** 3526-3531 (2009).

33. Kooij, E. S. & Vanmaekelbergh, D. Catalysis and pore initiation in the anodic dissolution of silicon in HF. *J. Electrochem. Soc.* **144,** 1296 (1997).

35. Kolasinski, K. W., Barclay, W. B., Sun, Y. & Aindow, M. The stoichiometry of metal assisted etching (MAE) of Si in V_2O_5+HF and HOOH+HF solutions. *Electrochim. Acta* **158,** 219 (2015).

36. Neuwald, U., Feltz, A., Memmert, U. & Behm, R. J. Chemical oxidation of hydrogen passivated Si (111) surfaces in H_2O_2. *J. Appl. Phys.* **78,** 4131 (1995).

37. Gondek, C., Lippold, M., Röver, I., Bohmhammel, K. & Kroke, E. Etching silicon with HF-H_2O_2-based mixtures: reactivity studies and surface investigations. *J. Phys. Chem., C* **118,** 2044 (2014).

FIGURES

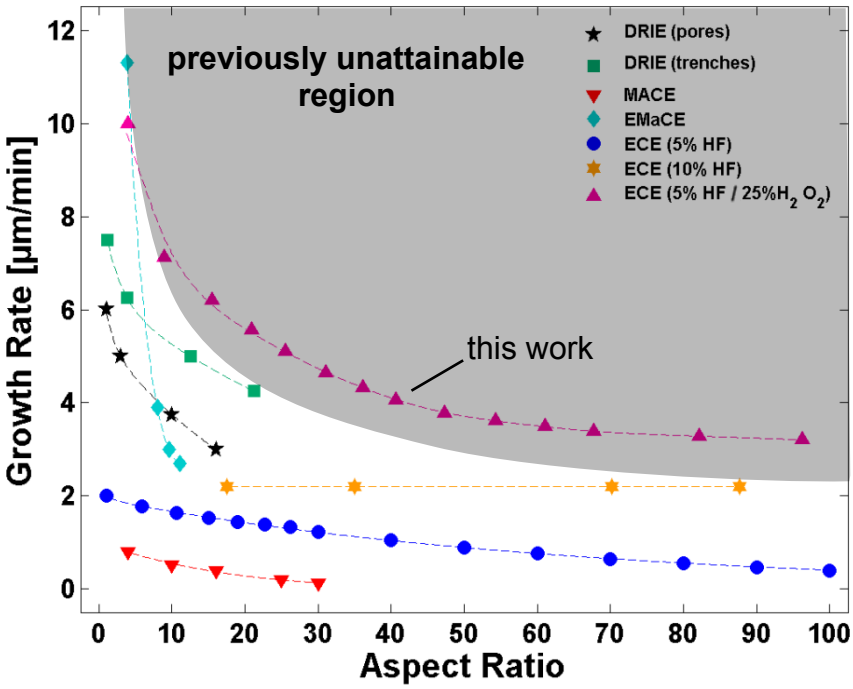

Figure 1

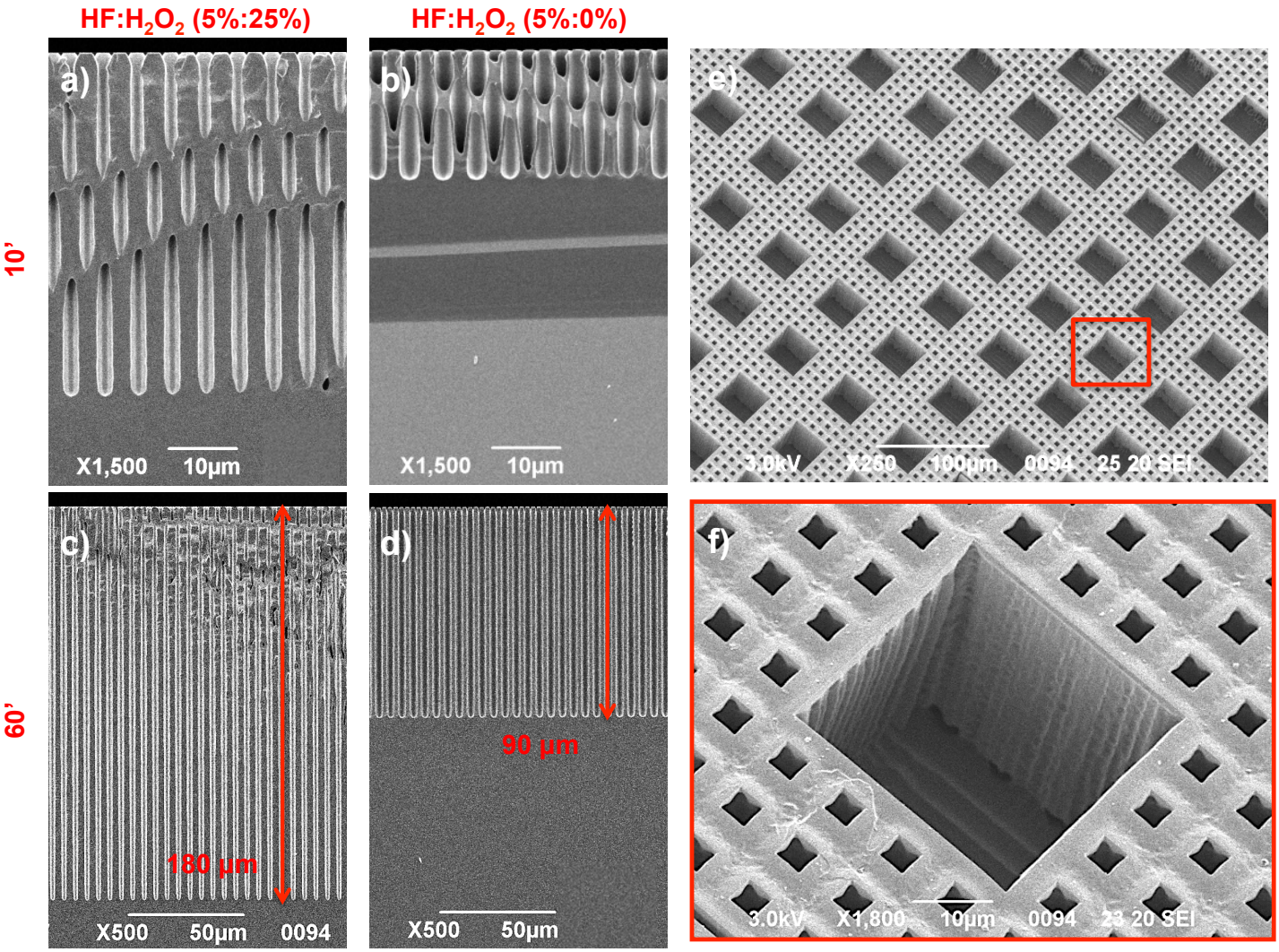
HF:H2O2 (5%:25%)
HF:H2O2 (5%:0%)
10'
60'
a)
X1,500 10µm
b)
X1,500 10µm
e)
3.0kV X250 100µm 0094 25 20 SEI
c)
180 µm
X500 50µm 0094
d)
90 µm
X500 50µm
f)
3.0kV X1,800 10µm 0094 23 20 SEI

Figure 2

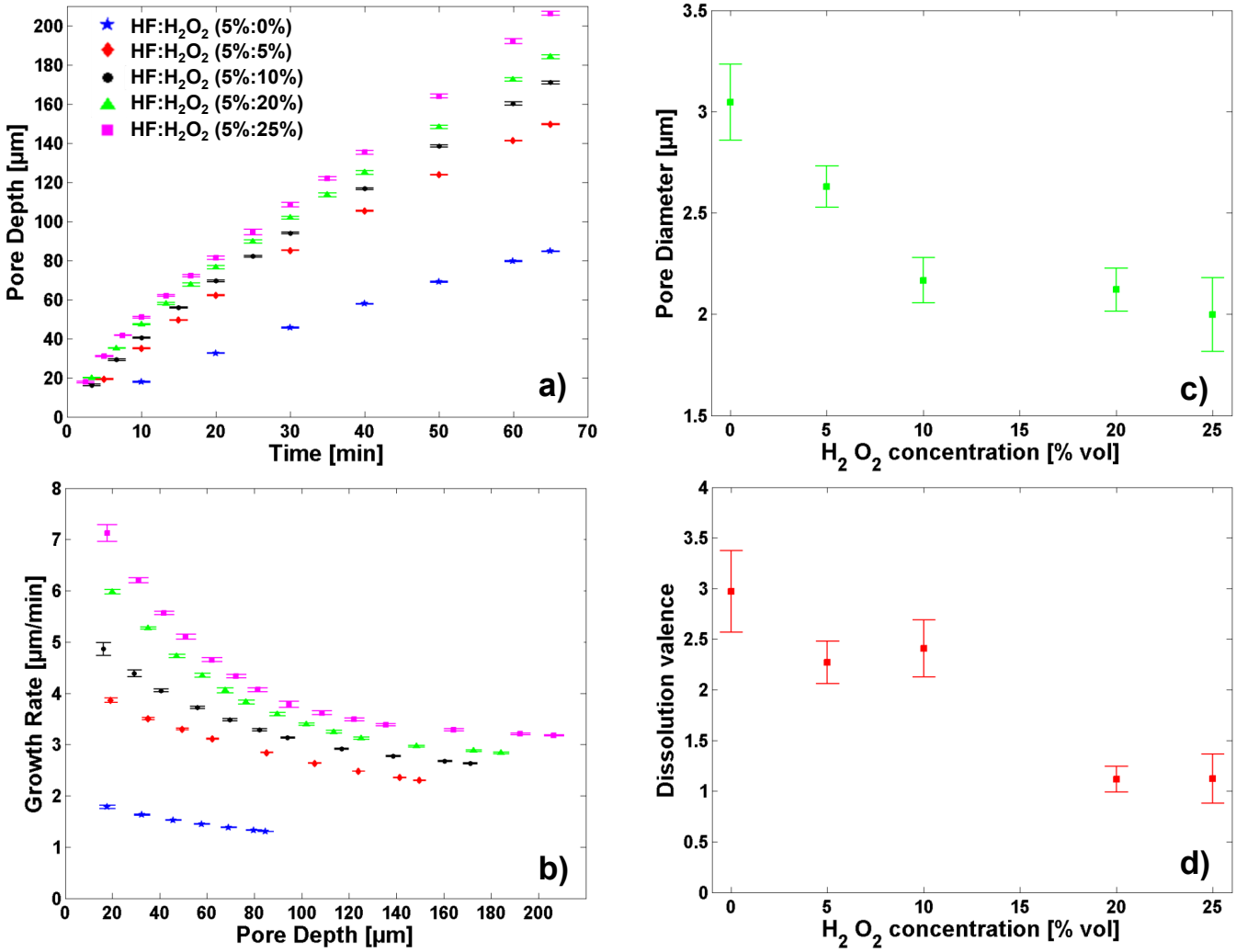
HF:H2O2 (5%:0%)
HF:H2O2 (5%:5%)
HF:H2O2 (5%:10%)
HF:H2O2 (5%:20%)
HF:H2O2 (5%:25%)
Pore Depth [µm]
Time [min]
a)
Pore Diameter [µm]
H2 O2 concentration [% vol]
c)
Growth Rate [µm/min]
Pore Depth [µm]
b)
Dissolution valence
H2 O2 concentration [% vol]
d)

Figure 3

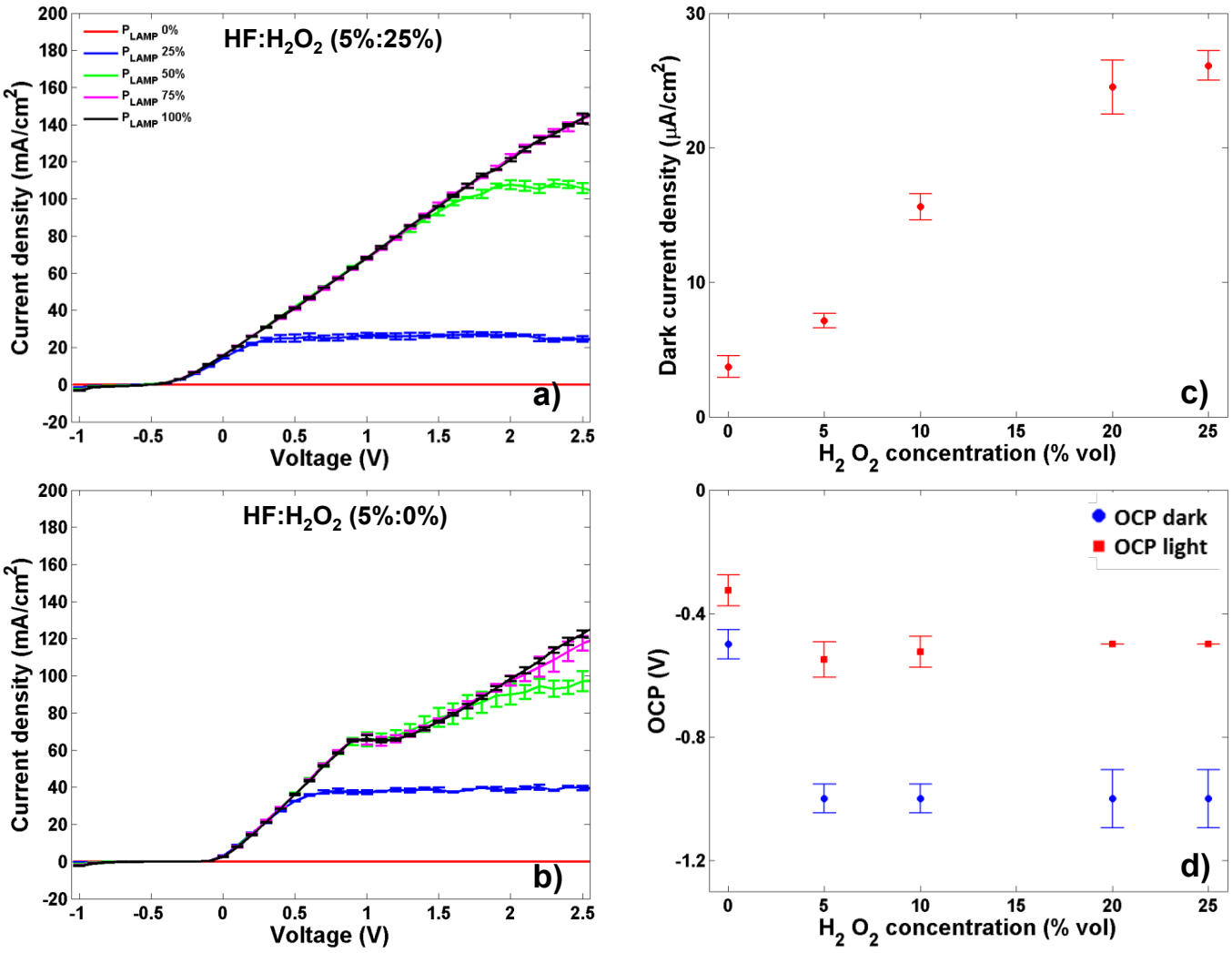
HF:H2O2 (5%:25%)
PLAMP 0%
PLAMP 25%
PLAMP 50%
PLAMP 75%
PLAMP 100%
Current density (mA/cm2)
Voltage (V)
a)
HF:H2O2 (5%:0%)
Current density (mA/cm2)
Voltage (V)
b)
Dark current density (μA/cm2)
H2O2 concentration (% vol)
c)
OCP dark
OCP light
OCP (V)
H2O2 concentration (% vol)
d)

Figure 4

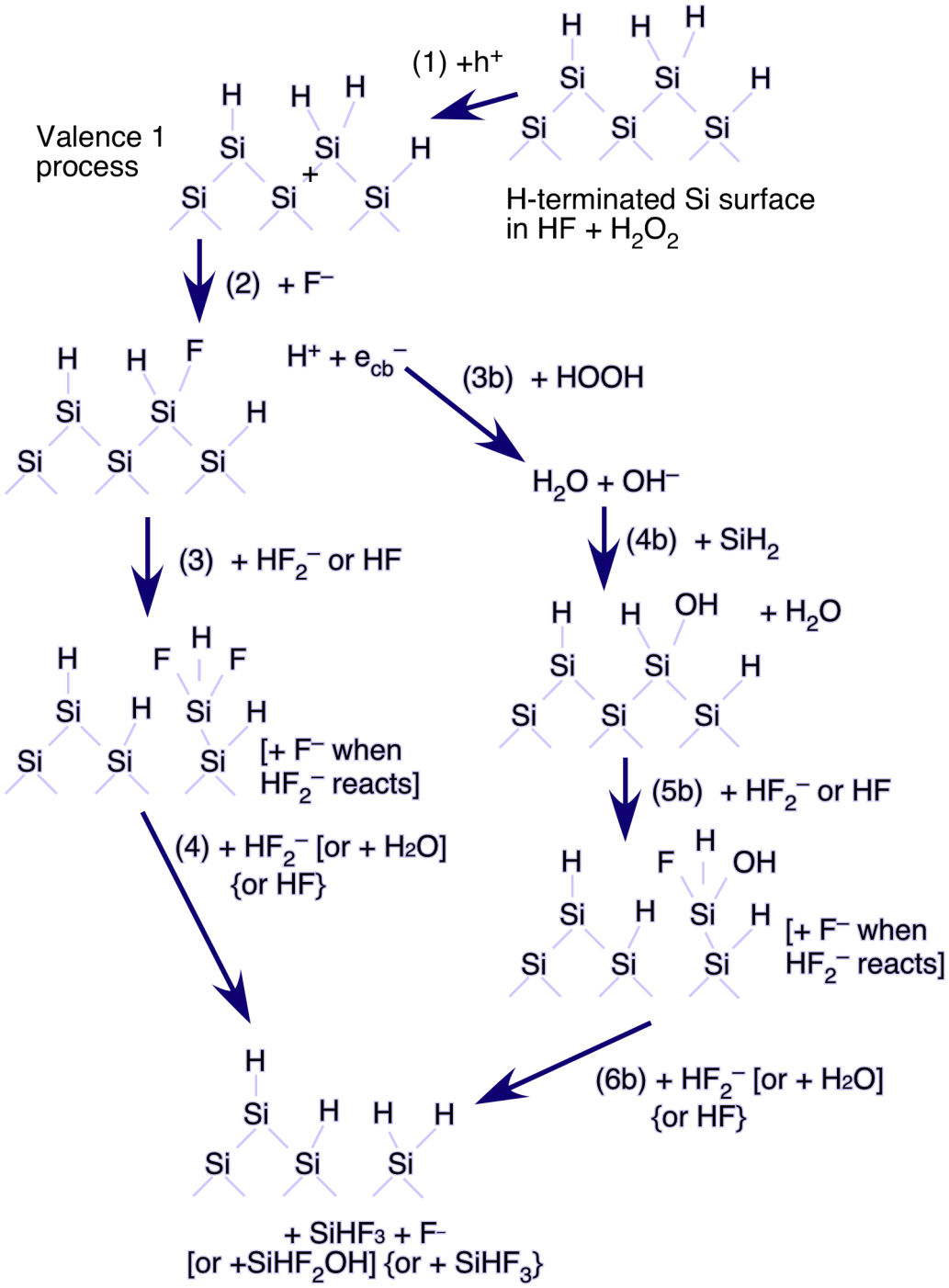
(1) +h+
Valence 1 process
H-terminated Si surface in HF + H2O2
(2) + F−
H+ + ecb−
(3b) + HOOH
H2O + OH−
(4b) + SiH2
(3) + HF2− or HF
+ H2O
[+ F− when HF2− reacts]
(5b) + HF2− or HF
(4) + HF2− [or + H2O] {or HF}
[+ F− when HF2− reacts]
(6b) + HF2− [or + H2O] {or HF}
+ SiHF3 + F−
[or +SiHF2OH] {or + SiHF3}

Figure 5

CAPTIONS

Figure 1: Figure of merit of main silicon micromachining technologies. Comparison between this work and commercial/state-of-art silicon microfabrication technologies, namely Deep Reactive Ion Etching (DRIE) [10], Metal Assisted Chemical Etching (MaCE) [12, 13], Elecric bias-attenuated MaCE (EMaCE) [14], Electrochemical Etching (ECE) at [HF] of 5 and 10% [20], in term of growth rate (ratio between etch depth and etch time [μm/min]) versus aspect-ratio (ratio between the depth of in-silicon vertical feature and its width). The figure highlight as this work allows silicon microfabrication entering the previously unattainable region for aspect ratio values in the range 10-100.

Figure 2: Effect of the addition of H_2O_2 to HF-aqueous electrolyte on the fabrication of regular macropore arrays in silicon by electrochemical etching. SEM cross-section of regular macropore arrays etched under back-side illumination for 10 (a, b) and 60 minutes (c, d) at 1.2 V and etching current density of 36.49 mA/cm^2 in the presence of [HF]=5%-based electrolyte with [H_2O_2] = 25% (a, c) and without H_2O_2 (reference) (b, d). It is appreciable the significant increase of the etching rate by addition of H_2O_2 to the reference electrolyte. (e, f) SEM bird-views of a silicon microstructure that integrates a 2D array of holes with depth of 50 μm and different aspect-ratios (namely, 1 and 10) on the same silicon die, fabricated in 10 minutes at 3 V and 60 mA/cm^2 in the presence of [HF]=5%-based electrolyte with [H_2O_2] = 25%. Noteworthy, the possibility of control the etching anisotropy in real-time and fabricate complex microstructures is retained at high etching rates.

Figure 3: Effect of the H_2O_2 concentration within HF-aqueous electrolyte on pore depth and growth rate of regular macropore arrays fabricated in silicon by electrochemical etching. Experimental data on depth (average value and standard deviation) versus time (a) and growth rate (average value and standard deviation) versus depth (b) of regular macropore arrays etched at 1.2 V and etching current density of 36.49 mA/cm^2 in the presence of [HF] = 5%-based electrolyte with different H_2O_2 concentrations (i.e. 0, 5, 10, 20, 25%); experimental data on pore diameter (c) and dissolution valence (d) of regular macropore arrays, etched in the same conditions above reported, as a function of the [H_2O_2] concentration. Remarkably, the dissolution valence of pores etched in the presence of H_2O_2 at concentration of 25% is lowered to 1.

Figure 4: Investigation of the effect of H_2O_2 concentration within HF-aqueous electrolyte on the silicon dissolution process. Experimental current density-voltage curves (average value and standard deviation) of *n*-type silicon electrode in the presence of two different [HF] = 5%-based electrolytes with [H_2O_2]=25% (by vol.) (a) and without H_2O_2 (reference) (b), both in dark and under back-side illumination; current density value in dark (c) and open-circuit potential value (d) as a function of the [H_2O_2] concentration, both in dark and under illumination of the silicon electrode.

Figure 5: A schematic representation of the standard Gerischer mechanism augmented by H_2O_2 assisted etching of Si. The series of steps along the left hand column corresponds to the Gerischer mechanism. Etching is always initiated by hole injection into the valence band. However, in the presence of H_2O_2, a second etching pathway opens up (the right hand pathway) in which the electron injected

into the conduction band by F^- is captured by H_2O_2. This liberates OH^- at the surface, which induces further etching through base-catalyzed hydrolysis. Both reactions, when performed separately, are known to yield hydrogen-terminated surfaces after Si atom removal.

SUPPORTING INFORMATION

Controlled Electrochemical Etching of High-Aspect-Ratio Structures in Silicon at the Highest Etching Rates: The Role of H_2O_2 in the Anodic Dissolution of Silicon in Acidic Electrolytes

C. Cozzi[1], G. Polito[1], K.W. Kolasinski[2] and G. Barillaro*[1]

[1] Dipartimento di Ingegneria dell'Informazione, Università di Pisa, via G. Caruso 16, 56122 Pisa, Italy

[2] Department of Chemistry, West Chester University, West Chester, PA 19383 USA

*g.barillaro@iet.unipi.it

Electrochemical etching setup

The electrochemical etching setup includes a three-electrode PTFE (Polytetrafluoroetylene) cylindrical cell having a volume of 400 cm^3. A circular window (0.64 cm^2) in the electrochemical cell wall allows the front side of the silicon sample (anode) to be in contact with the electrolyte solution, which is continuously stirred during both the electrochemical characterization and etching. Back side illumination of the sample is performed with a 250 W halogen lamp (Osram Xenophot 64653 HLX), positioned about 6 cm apart from the sample, through a sapphire circular window (0.64 cm^2) in the metal electrode used to provide the electrical contact to the sample. An IR filter with a cutoff wavelength

of 750 nm is placed between the lamp and the silicon sample in order to avoid carrier generation close to the silicon surface in contact with the electrolyte. The lamp power and, in turn, the illumination intensity are finely tuned through a feedback loop, performed by using a PID controller (Eurotherm 2604), which supplied also a second feedback loop thus allowing the working temperature to be maintained at 22 °C. The electrochemical cell includes both a cathode, consisting of a platinum disc (0.64 cm^2) placed in front of the silicon anode at a distance of 1 cm, and a pseudo-reference wire electrode close to the silicon electrode, at a distance of about 2 mm, made of platinum. A Source Measure Unit (Keithley 2410 Source Meter) is used to apply a voltage between the silicon anode and the pseudo-reference electrode (platinum wire) and to monitor the current flowing between the silicon anode and the cathode (platinum disc).

Macropore labeling methodology

The labeling methodology is based on the pulse modulation of the etching current density over time, which requires periodic increases of the etching current density with a pulse to a higher labeling value, with respect to the working value, so as to mark the macropore at given times along its depth with higher porosity regions. The current density pulse must be short enough to avoid perturbation of the growth rate during the etching, on the one hand, and long enough to label the pore with a visible marker, on the other hand. This is achieved by using a current density pulse producing a porosity variation of 10%, with respect to the working value. The duration of each current density pulse is set to 30 s for the reference electrolyte and to 15 s for electrolytes containing H_2O_2 solutions, which give rise

to a marker of about 1.5 μm in width. The silicon etching lasted 65 min (3900 s) and the time between one marker and the next one is in the range from 135 s and 585 s. Its value depends on both electrolyte solution composition (i.e. H_2O_2 concentration) and pore depth during the etching [23].

In order to clarify the labeling methodology here above reported, Figure S1 shows the graph of the time-pulse modulation of etching current density used to label macropores etched in the HF-based electrolyte with $[H_2O_2]$ = 5% and the Optical Microscope cross-section of the resulting macropore arrays. It is apparent that each marker along the macropore depth (m*i*, with *i*=1,2,..8, in Figure S1b) corresponds to the current density pulse (m*i*) with the same index *i*, which is a rectangular wave (insert in Figure S1a).

FIGURES

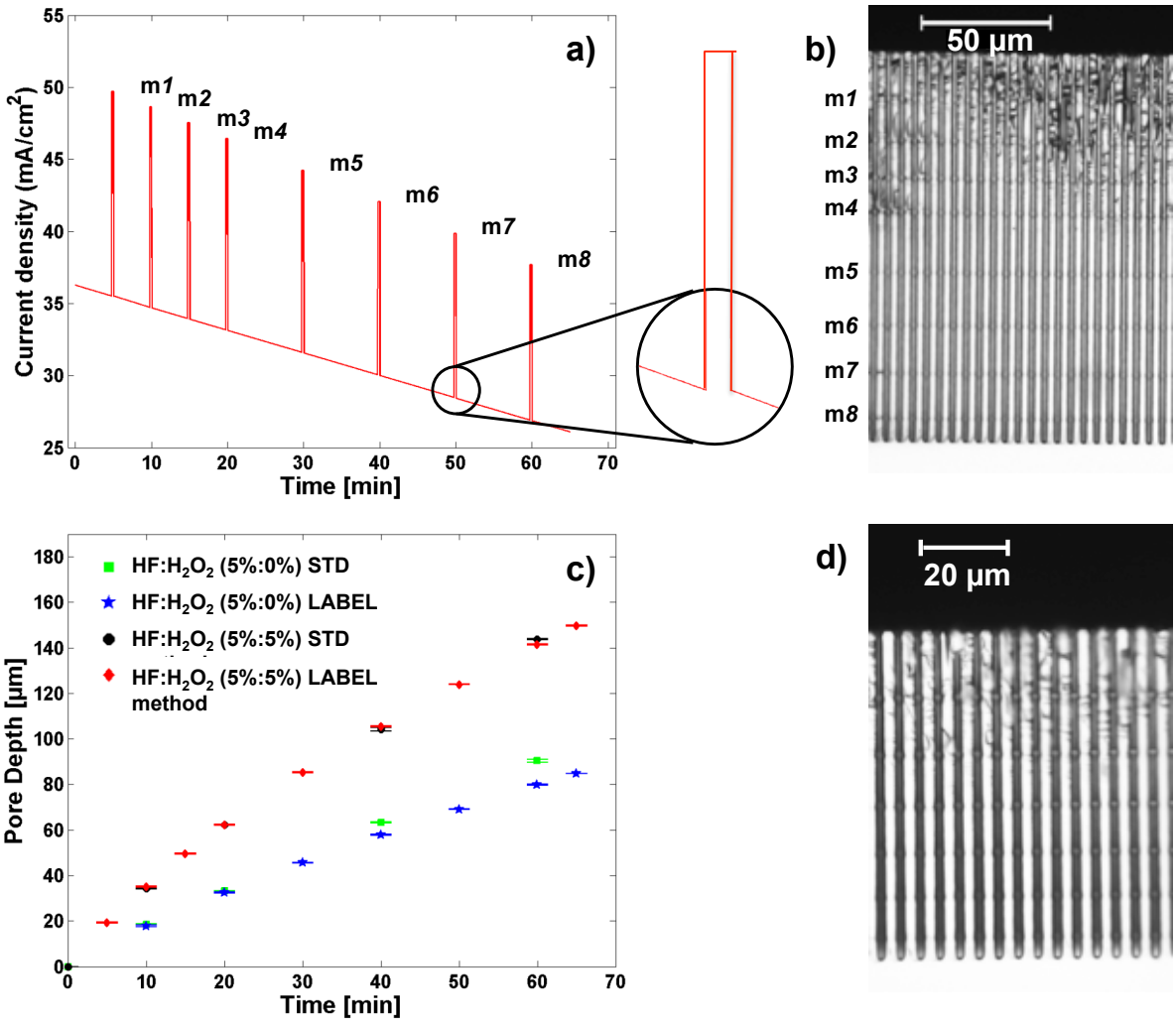

Figure S1

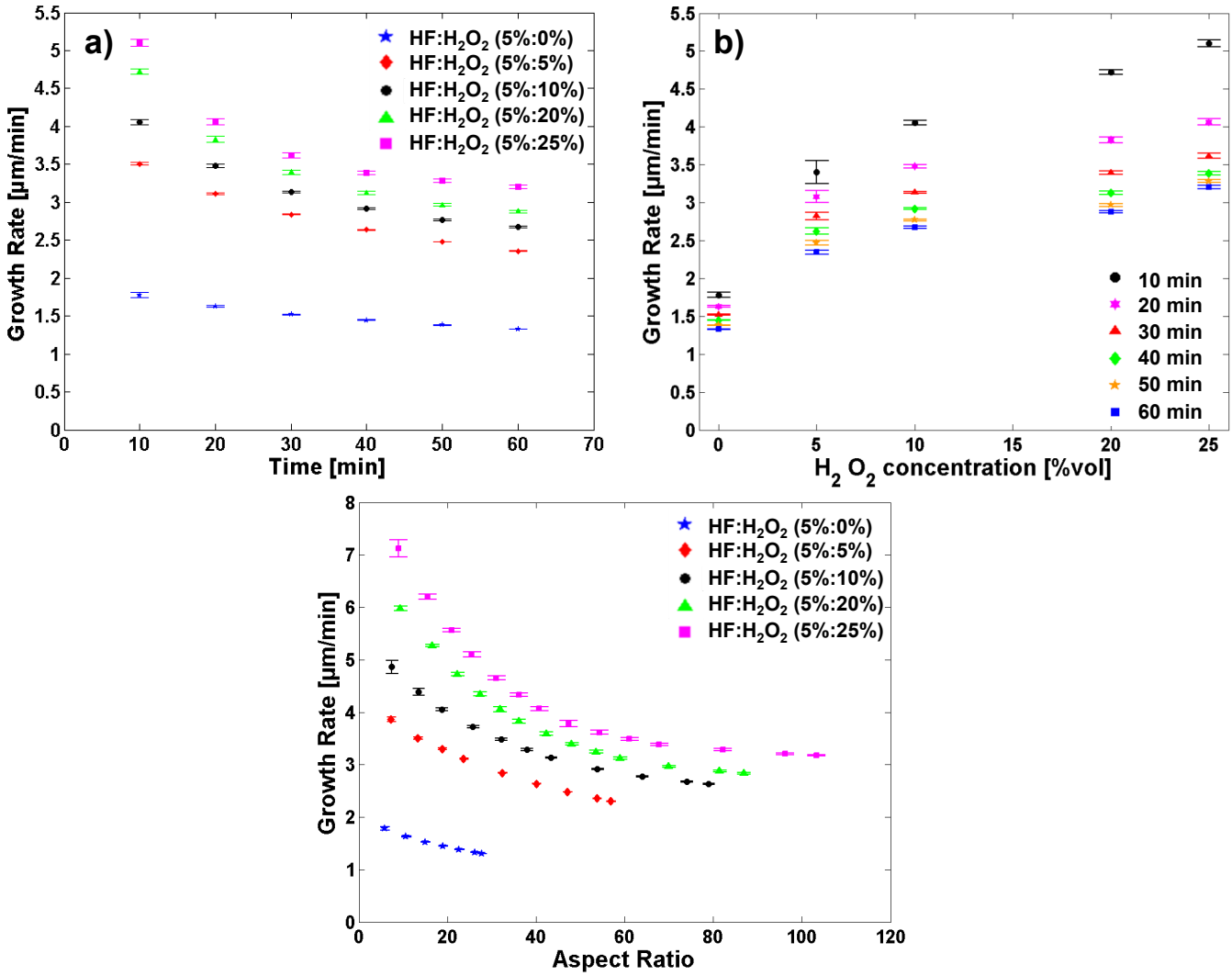
a)
HF:H2O2 (5%:0%)
HF:H2O2 (5%:5%)
HF:H2O2 (5%:10%)
HF:H2O2 (5%:20%)
HF:H2O2 (5%:25%)
Growth Rate [µm/min]
Time [min]
b)
10 min
20 min
30 min
40 min
50 min
60 min
Growth Rate [µm/min]
H2 O2 concentration [%vol]
HF:H2O2 (5%:0%)
HF:H2O2 (5%:5%)
HF:H2O2 (5%:10%)
HF:H2O2 (5%:20%)
HF:H2O2 (5%:25%)
Growth Rate [µm/min]
Aspect Ratio

Figure S2

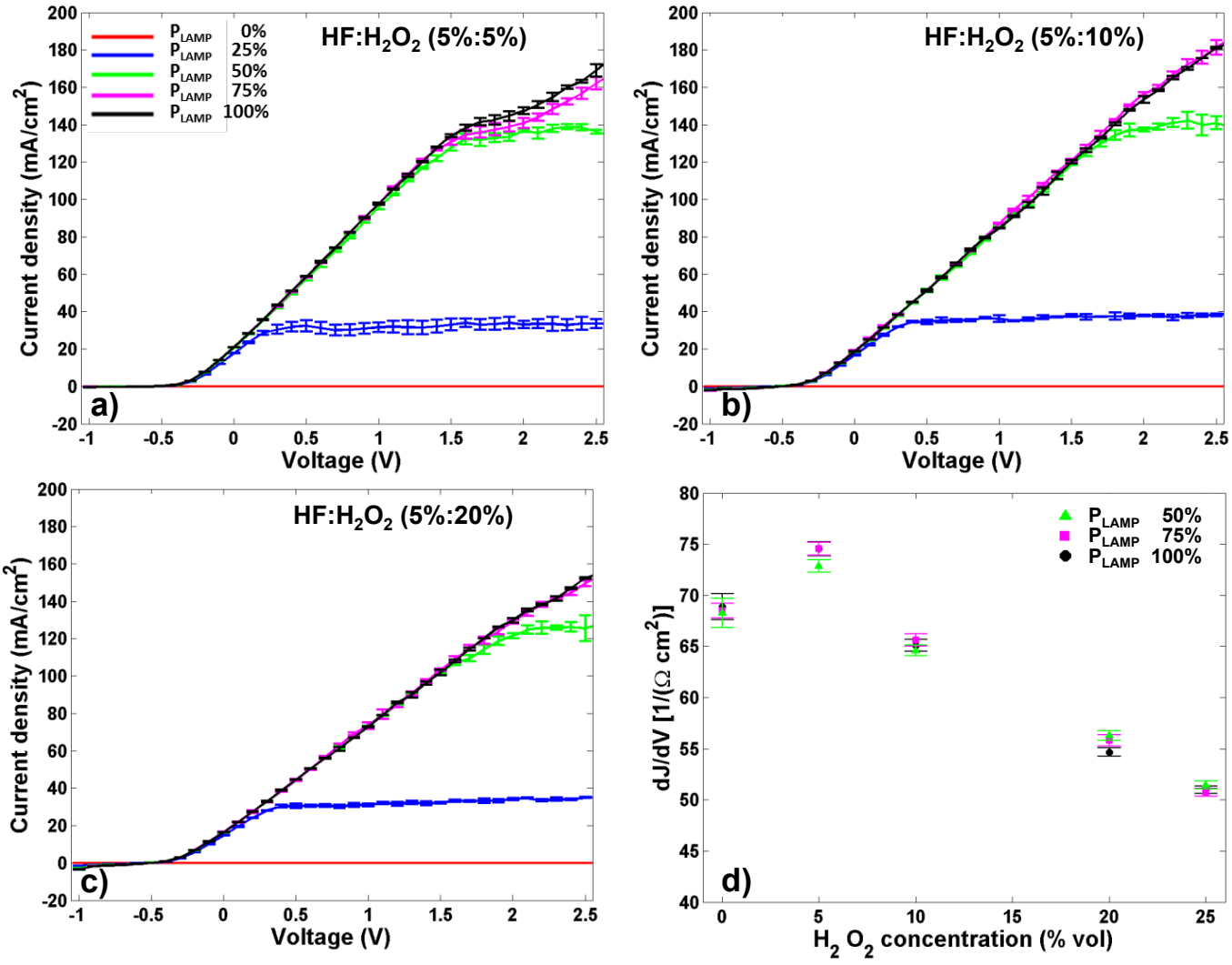
HF:H2O2 (5%:5%)
HF:H2O2 (5%:10%)
HF:H2O2 (5%:20%)
PLAMP 0%
PLAMP 25%
PLAMP 50%
PLAMP 75%
PLAMP 100%
Current density (mA/cm2)
Voltage (V)
a)
b)
c)
d)
dJ/dV [1/(Ω cm2)]
H2 O2 concentration (% vol)

Figure S3

CAPTIONS

Figure S1: Labeling of regular macropore arrays over depth. Time-pulse modulation of etching current density used to label macropores etched in a [HF]=5%-based electrolyte with [H_2O_2] = 5% (a); optical microscope cross-section images of ordered macropore arrays etched under back-side illumination by means of labeling methodology for 65 minutes at 1.2 V and 36.49 mA/cm^2 in the presence of [H_2O_2] = 5% (b) and [H_2O_2]=0% (reference) (d); (c) labeling methodology validation by comparison of experimental data on depth (average value and standard deviation) of regular macropore arrays etched at 1.2 V and 36.49 mA/cm^2 up to 65 minutes by means of both labeling (blue stars and red diamonds) and standard (green squares and black circles) methodologies in a [HF]=5%-based electrolyte with [H_2O_2] = 5% and [H_2O_2]=0% (reference).

Figure S2: Growth rate versus time, H_2O_2 concentration, and aspect ratio of regular macropore arrays fabricated in silicon using a [HF]=5%-based electrolyte with different [H_2O_2] concentration by electrochemical etching. Experimental data on growth rate (average value and standard deviation) versus time (a), H_2O_2 concentration (b), and aspect ratio (c) of regular macropores etched at 1.2 V and 36.49 mA/cm^2 in the above reported electrolyte by electrochemical etching.

Figure S3: Current density-voltage curves of *n*-type silicon electrode in the presence of [HF]=5%-aqueous electrolytes with different H_2O_2 concentrations (i.e. 5, 10, 20%) at different illumination intensities under back-side illumination. Experimental data (average value and standard deviation) of *J-V* curves for three different electrolytes above reported (a-c); (d) slope of experimental *J-V* curves

(dJ/dV) as a function of H_2O_2 concentration, estimated from the linear region beyond 0 V under high illumination intensity (≥50% of the lamp power).